

Constraining the Milky Way's Dispersion Measure Using FRB and X-ray Data

Jiale Wang ¹ , Zheng Zhou ¹ , Xiaochuan Jiang ² , Taotao Fang ^{1,*} 

¹ Department of Astronomy, Xiamen University, Xiamen 361005, China; wangjiale@stu.xmu.edu.cn (J.W.); zhengz@stu.xmu.edu.cn (Z.Z.)

² School of Information Engineering, Fujian Business University, Fuzhou 350506, China; jiangxc@xmu.edu.cn

* Correspondence: fangt@xmu.edu.cn

Abstract: The dispersion measures (DMs) of the fast radio bursts (FRBs) are a valuable tool to probe the baryonic content of the intergalactic medium and the circumgalactic medium of the intervening galaxies along the sightlines. However, interpreting the DMs is complicated by the contribution from the hot gas in and around our Milky Way. This study examines the relationship between DM_{MW} , derived from localized FRBs, and the Galaxy's hot gas, using X-ray absorption and emission data from O VII and O VIII. We find evidence for a positive correlation between DM_{MW} and O VII absorption, reflecting contributions from both the disk and halo components. This conclusion is supported by two lines of evidence: (1) No correlation between DM_{MW} and O VII/O VIII emission, which primarily traces dense disk regions; and (2) the comparison with electron density models, where DM_{MW} aligns with models that incorporate both disk and halo components but significantly exceeds predictions from pure disk-only models, emphasizing the halo's role. Furthermore, the lack of correlation with O VIII absorption suggests that the primary temperature of the Galaxy's hot gas is likely around 2×10^6 K or less, as traced by O VII absorption, while gas at higher temperatures ($\sim 3 - 5 \times 10^6$ K) is present but less abundant. Our findings provide insights into the Milky Way's gas distribution and improve DM_{MW} estimates for future cosmological studies.

Keywords: Galaxy: halo; X-rays: diffuse background; radio continuum: transients

1. Introduction

Fast Radio Bursts (FRBs) are intense, millisecond-duration radio pulses originating from extragalactic sources [1]. They often exhibit high dispersion measures (DM), which reflect the integrated electron density along their line of sight. This makes FRBs invaluable tools for probing baryon density across the universe, including addressing the “missing baryon” problem, where a significant fraction of baryons at low redshifts are believed to be undetected [2]. These baryons are thought to exist in the form of diffuse, hot gas within the Intergalactic Medium (IGM) and the Circumgalactic Medium (CGM) of intervening galaxies, which are challenging to observe directly due to their high temperatures, low densities, and the limitations of current telescopes [3–5]. By using FRBs to trace the distribution of ionized baryons, we can gain insights into these otherwise elusive components of the universe.

One of the primary challenges in using FRBs for cosmological studies is accurately determining the Milky Way (MW) contribution to the observed DM (DM_{MW}). The total observed DM of an FRB can be expressed as [6]:

$$DM_{\text{obs}} = \frac{DM_{\text{Host}}}{1+z} + DM_{\text{IGM}} + DM_{\text{MW,disk}} + DM_{\text{MW,halo}}. \quad (1)$$

Academic Editor: Eric Schlegel

Received: 18 December 2024

Revised: 22 January 2025

Accepted: 25 January 2025

Published:

Citation: Wang, J.; Zhou, Z.; Jiang, X.; Fang, T. Constraining the Milky Way's Dispersion Measure Using FRB and X-ray Data. *Universe* **2025**, *1*, 0. <https://doi.org/>

Copyright: © 2025 by the authors. Submitted to *Universe* for possible open access publication under the terms and conditions of the Creative Commons Attribution (CC BY) license (<https://creativecommons.org/licenses/by/4.0/>).

Here, DM_{Host} represents the contribution from the host galaxy, scaled by its redshift (z), DM_{IGM} is the contribution from the intergalactic medium, $DM_{\text{MW,disk}}$ represents the contribution from the Milky Way disk, and $DM_{\text{MW,halo}}$ represents the contribution from the Milky Way halo. The sum of $DM_{\text{MW,disk}}$ and $DM_{\text{MW,halo}}$ represents the total contribution from the Milky Way, DM_{MW} . In most previous studies, this total MW contribution has been modeled using a disk component (modeled by NE2001 or YMW16 [see, 7,8]) plus an assumed constant $DM_{\text{MW,halo}}$ to account for the halo component.

However, this approach can introduce significant uncertainties. The disk and halo components of the Milky Way are highly complex, with the gas distribution being neither uniform nor well-constrained. Simply adding a constant value for the halo contribution overlooks variations in density, temperature, and geometry, leading to potential under- or overestimation of DM_{MW} . Furthermore, the NE2001 and YMW16 models, widely used for Galactic electron density studies, show limitations in high-latitude regions, produce significant discrepancies in certain directions, and exhibit notable biases when compared to independent pulsar distance measurements, leading to estimation errors in FRB studies [9]. As a result, this method can lead to significant inaccuracies in determining the Milky Way's DM contribution, which directly impacts our ability to accurately isolate and study the IGM and CGM components [see, 10,11].

These uncertainties have prompted various studies to place constraints on $DM_{\text{MW,halo}}$ using FRBs. Platts et al. [12] first established conservative constraints on $DM_{\text{MW,halo}}$ by analyzing a population of FRBs and adjusting for $DM_{\text{MW,disk}}$ as computed by the NE2001 model. Their analysis suggested a wide range for $DM_{\text{MW,halo}}$, between -2 and 123 pc cm^{-3} , to account for potential uncertainties. Following this, Cook et al. [13] refined these estimates using the CHIME/FRB dataset, establishing $DM_{\text{MW,halo}}$ upper limits between 52 and 111 pc cm^{-3} for Galactic latitudes $|b| \geq 30^\circ$. More recently, Wei and Melia [14] analyzed DM and redshift data from 24 localized FRBs to explore cosmological models. By applying a flat prior for $DM_{\text{MW,halo}}$ ranging from 5 to 80 pc cm^{-3} , they yielded a Hubble constant of $H_0 = 95.8_{-7.8}^{+9.2} \text{ km s}^{-1} \text{ Mpc}^{-1}$, highlighting the potential of FRBs to contribute to cosmological parameter estimation. In the latest study, Huang et al. [15] employed cosmological hydrodynamical simulations of the Local Universe to construct a DM model encompassing the Milky Way halo, the Local Group (including contributions from the intra-group medium), and the broader Local Universe (up to 120 Mpc). They reported an average value of $DM_{\text{MW,halo}}$ of 46 pc cm^{-3} with a standard deviation of 17 pc cm^{-3} . These variations in $DM_{\text{MW,halo}}$ are particularly critical, as the halo component contributes significantly to the overall DM_{MW} budget and directly affects our ability to isolate the IGM contribution. Therefore, understanding and constraining $DM_{\text{MW,halo}}$ more accurately is crucial for reducing uncertainties in the IGM and CGM components, which are key to our understanding of the large-scale structure of the universe.

In this work, we focus on studying the total DM_{MW} , considering the combined contributions from both the disk and halo components. The Milky Way's hot gas, with a temperature of a few million degrees, is ideal for producing highly ionized species such as O VII and O VIII [16,17]. While directly tracing electron density is challenging, these ions serve as effective tracers of the hot, highly ionized gas, as demonstrated by numerous X-ray observations [18]. By analyzing O VII and O VIII emission and absorption data, we aim to establish correlations between these X-ray tracers and the overall DM_{MW} . This approach will help reduce uncertainties in the Milky Way DM contribution, thereby enhancing the utility of FRBs as cosmological probes. It can also help improve our understanding of the ionized gas distribution within the MW.

The structure of this paper is as follows: In Section 2, we present a list of localized FRBs and describe the method used to calculate DM_{MW} . Section 3 focuses on the relationship

between FRBs and key Galactic gas tracers, including X-ray O VII and O VIII data. In Section 4, we discuss the observed correlations and compare them with existing MW electron distribution models, and the last section provides a summary.

2. Data and Methods

2.1. Localized FRBs Sample

Our FRB data were obtained from the Blinkverse Database [19], which provides a comprehensive and up-to-date collection of FRB observations from various observatories, including FAST, CHIME, GBT, and Arecibo. To identify localized FRBs with known redshifts, we searched for each event in the database using the Astrophysical Data Service (ADS) [20]. This process resulted in a sample of 47 localized FRBs, which are listed in Table 1 and shown in their sky distribution and as a function of redshift in Figure 1.

2.2. Derivation of DM_{MW}

Based on the observed DM values (DM_{obs}) of 47 localized FRBs, we derived DM_{MW} by subtracting DM_{IGM} , estimated using average values from the Macquart relation [see, 6], and DM_{host} , assumed to be $30/(1+z)$ pc cm⁻³ to account for redshift z , consistent with results from the Illustris-1 simulation, where Mo et al. [21] reported a median DM_{host} value of 31 pc cm⁻³ in their stellar mass model. DM_{MW} was derived based on Equation 1.

To account for possible higher DM_{host} values, we also tested assumptions of DM_{host} up to 60 pc cm⁻³ and 100 pc cm⁻³. These alternative values were included in the calculations, and while the detailed results are presented as Alternative 1 and 2 in Table 2, we emphasize that the choice of $DM_{host} = 30$ pc cm⁻³ does not qualitatively affect our findings.

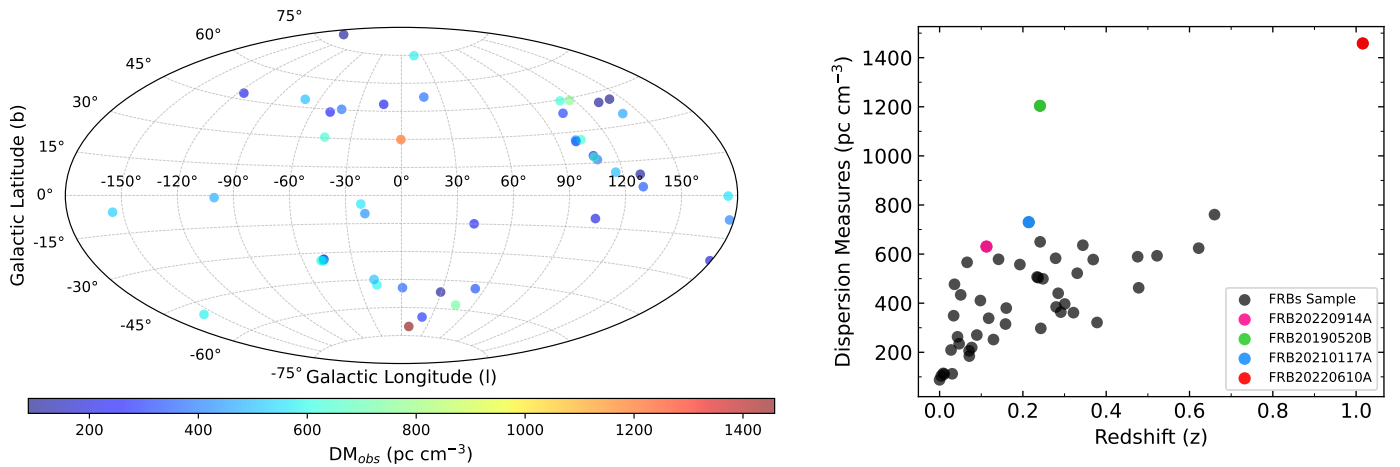


Figure 1. Left: Sky distributions in celestial coordinates of 47 localized FRBs analyzed in this work. The color represents the magnitude of their observed DM (DM_{obs}). Right: DM as a function of redshift for these FRBs, with four unusually high- DM FRBs highlighted.

Notably, this approach yielded unusually high DM_{MW} values (exceeding 500 pc cm⁻³) for FRB 190520B, FRB 210117A, FRB 220610A, and FRB 220914A. Since these FRBs are located at Galactic latitudes above 15 degrees, where the Milky Way's contribution should be minimal, the observed DM_{MW} values far exceed expectations, suggesting significant additional DM contributions from their host galaxies. Consequently, we consulted localization studies for these FRBs and subtracted the host galaxy DM values reported: FRB 190520B [22], FRB 210117A [23], FRB 220610A [24], and FRB 220914A [25]. For FRB 220610A, we also adopted the DM_{IGM} value provided in its respective study to avoid a negative DM_{MW} outcome. Importantly, we note that our main results do not rely on the special treatment of these four FRBs.

To ensure that our main findings are not influenced by the special treatment of these four FRBs, we conducted two additional analyses. First, for all localized FRBs, if a DM_{host} value was reported in their localization papers, we adopted that value; otherwise, we used $30/(1+z)$ pc cm⁻³. Second, we excluded these four FRBs entirely from the sample. Both results are presented as Alternative 3 and 4 in Table 2, demonstrating that our findings remain robust and are not dependent on the special treatment applied to these four unusual FRBs.

Additionally, a negative DM_{MW} was obtained for FRB 190611B, suggesting that the FRB's signal may have traversed regions of significantly low density or voids, resulting in a DM_{IGM} much lower than the average predicted by the Macquart relation, or that the association between this FRB and its host galaxy may need to be re-examined and redefined, as suggested by Cordes et al. [26]. However, since the presence of this data does not affect our main conclusions, we chose to retain it in our study.

3. Analysis and Findings

Currently, X-ray observations provide one of the most effective methods to study the hot gas distribution in and around the Milky Way, particularly through the detection of O VII and O VIII absorption and emission lines, which are sensitive to the temperature and density of gas in the Galactic disk and halo. In this section, we compare our DM_{MW} sample with these X-ray tracers to investigate potential correlations and the role they play in mapping the hot gas content of the Milky Way.

3.1. O VII Absorption

In this subsection, we analyze the relationship between DM_{MW} and O VII absorption lines, which trace hot gas in both the Galactic disk and halo, using active galactic nuclei (AGN) as background sources. We used the dataset from Fang et al. [48] but excluded the source Mkn 841, as its O VII absorption line equivalent width significantly exceeds typical Galactic levels and is likely contaminated, as suggested by Longinotti et al. [49].

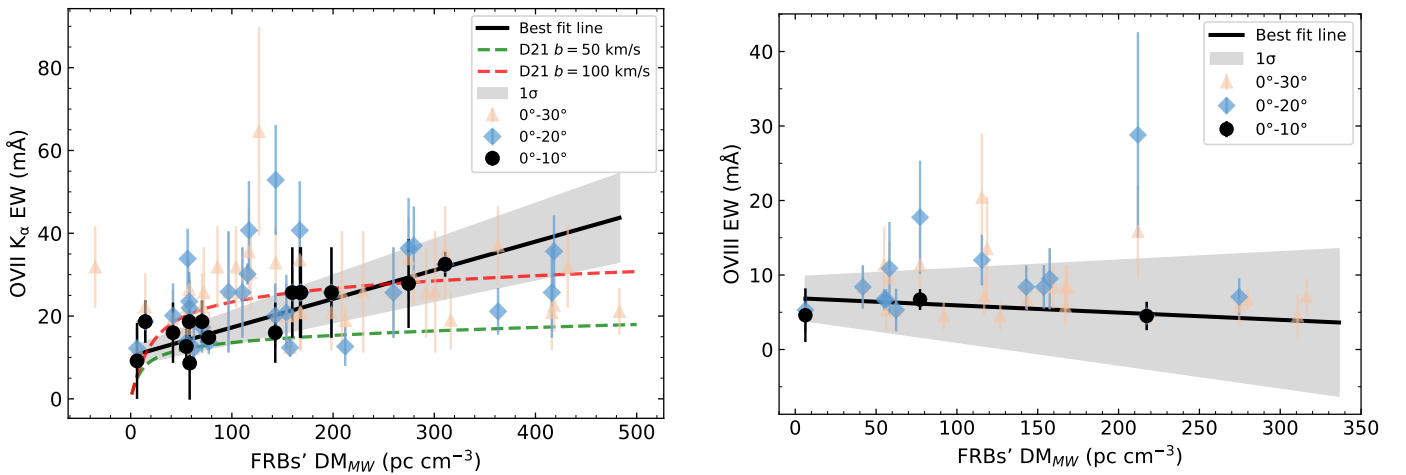


Figure 2. The correlation between DM_{MW} and the equivalent width (EW) of O VII (left) and O VIII (right) absorption lines. For each FRB, black circles, blue squares, and light orange triangles represent the average equivalent width of sources found within 10, 20, and 30-degree angular regions centered on the FRB's Galactic coordinates (l, b). The solid lines show the best-fit results obtained from the 10-degree region data for both O VII and O VIII using MCMC fitting, with shaded regions representing the 1σ uncertainties. In the left panel, the green and red dashed lines correspond to Doppler parameters $b = 50$ km/s and 100 km/s, respectively, based on the empirical formula derived by Das et al. [50] (see Section 4.1 for details).

Table 1. Localized FRBs Sample

No.	FRB	Telescope	l	b	DM	z	DM_{MW}^1	Repeater?	Ref
(1)	(2)	(3)	(deg)	(deg)	(cm^{-3} pc)	(redshift)	(cm^{-3} pc)	(y/n)	(10)
1	FRB121102A	Arecibo	174.95	-0.223	570	0.1927	366.370	n	Tendulkar et al. [27]
2	FRB171020A	ASKAP	29.3	-51.3	114.1	0.0087	77.196	n	Lee-Waddell et al. [28]
3	FRB180301A	Parkes	204.412	-6.481	522	0.3304	208.734	y	Bhandari et al. [29]
4	FRB180916B	CHIME	129.71	3.73	350.2	0.0337	291.964	n	Marcote et al. [30]
5	FRB180924B	ASKAP	0.74247	-49.415	361.42	0.3214	56.274	n	Bannister et al. [31]
6	FRB181030A	CHIME	133.4	40.9	103.5	0.0038	70.480	y	Bhardwaj et al. [32]
7	FRB181112A	ASKAP	342.6	-47.7	589.27	0.4755	143.298	n	Prochaska et al. [33]
8	FRB181220A	CHIME	105.24	-10.73	209.4	0.02746	157.412	n	Bhardwaj et al. [34]
9	FRB181223C	CHIME	207.75	79.51	112.51	0.03024	58.275	n	Bhardwaj et al. [34]
10	FRB190102C	ASKAP	312.65	-33.49	363.6	0.2910	85.762	n	Macquart et al. [6]
11	FRB190418A	CHIME	179.3	-22.93	184.5	0.07132	96.660	n	Bhardwaj et al. [34]
12	FRB190520B *	FAST	359.67	29.91	1204	0.2410	91.810	n	Niu et al. [22]
13	FRB190523A	DSA-10	117.03	44	760.8	0.6600	142.884	n	Ravi et al. [35]
14	FRB190608B	ASKAP	53.21	-48.53	338.7	0.1178	211.982	n	Macquart et al. [6]
15	FRB190611B	ASKAP	312.94	-33.28	321.4	0.3780	-35.053	n	Macquart et al. [6]
16	FRB190711A	ASKAP	310.91	-33.9	593.1	0.5220	104.044	y	Macquart et al. [6]
17	FRB190714A	ASKAP	289.7	49	504	0.2365	274.609	n	Heintz et al. [36]
18	FRB191001A	ASKAP	341.3	-44.8	506.92	0.2340	279.734	n	Heintz et al. [36]
19	FRB191228A	ASKAP	20.8	-64.9	297.5	0.2430	62.368	n	Bhandari et al. [29]
20	FRB200120E	CHIME	142.19	41.22	87.82	-0.0001	57.817	y	Kirsten et al. [37]
21	FRB200430A	ASKAP	17.06	52.52	380.1	0.1600	217.390	n	Heintz et al. [36]
22	FRB200906A	ASKAP	202.4	-49.77	577.8	0.3688	229.724	n	Bhandari et al. [29]
23	FRB201123A	MeerKAT	340.23	-9.68	433.9	0.0507	363.022	n	Rajwade et al. [38]
24	FRB201124A	CHIME	177.6	-8.5	410.83	0.0979	300.862	y	Fong et al. [39]
25	FRB210117A *	ASKAP	45.79	-57.59	730	0.2140	54.991	n	Bhandari et al. [23]
26	FRB210320C	ASKAP	318.88	45.31	384.593	0.2797	116.857	n	Gordon et al. [40]
27	FRB210405I	MeerKAT	338.19	-4.59	566.43	0.0660	482.984	n	Driessen et al. [41]
28	FRB210410D	MeerKAT	312.32	-34.13	578.78	0.1415	431.925	n	Caleb et al. [42]
29	FRB210807D	ASKAP	39.81	-14.89	251.9	0.1293	115.436	n	Gordon et al. [40]
30	FRB211127I	ASKAP	311.99	43.56	234.83	0.0469	167.058	n	Glowacki et al. [43]
31	FRB211203C	ASKAP	314.43	30.47	636.2	0.3439	310.726	n	Gordon et al. [40]
32	FRB211212A	ASKAP	243.95	47.76	206	0.0707	118.672	n	Gordon et al. [40]
33	FRB220105A	ASKAP	18.84	74.68	583	0.2785	316.335	n	Gordon et al. [40]
34	FRB220207C	DSA-110	106.94	18.39	263	0.0430	198.376	n	Law et al. [44]
35	FRB220307B	DSA-110	116.24	10.47	499.328	0.2481	259.665	n	Law et al. [44]
36	FRB220310F	DSA-110	140.02	34.8	462.657	0.4780	14.413	n	Law et al. [44]
37	FRB220319D	DSA-110	129.18	9.11	110.95	0.0110	72.187	n	Ravi et al. [45]
38	FRB220418A	DSA-110	110.75	44.47	624.124	0.6220	41.809	n	Law et al. [44]
39	FRB220506D	DSA-110	108.35	16.51	396.651	0.3004	110.398	n	Law et al. [44]
40	FRB220509G	DSA-110	100.94	25.48	270.26	0.0894	167.399	n	Connor et al. [25]
41	FRB220610A *	ASKAP	8.87	-70.13	1458.1	1.0160	6.275	n	Ryder et al. [24]
42	FRB220825A	DSA-110	106.99	17.79	649.893	0.2414	416.178	n	Law et al. [44]
43	FRB220912A	CHIME	347.27	48.7	221.8	0.0771	126.832	y	Ravi et al. [46]
44	FRB220914A *	DSA-110	104.31	26.13	630.703	0.1125	159.697	n	Connor et al. [25]
45	FRB220920A	DSA-110	104.92	38.89	314.98	0.1582	153.784	n	Law et al. [44]
46	FRB221012A	DSA-110	101.14	26.14	440.36	0.2847	168.185	n	Law et al. [44]
47	FRB230718A	ASKAP	259.66	-1.03	477	0.0357	418.343	n	Glowacki et al. [47]

Notes: ¹Values derived in this study.* DM_{MW} values for these four FRBs are obtained from works dedicated to their localization.

The left panel of Figure 2 shows the correlation between the equivalent width of O VII absorption lines and DM_{MW} . For each FRB, we identified O VII absorption sources within 10, 20, and 30-degree angular regions centered on their respective sky positions in Galactic coordinates, represented by black circles, blue squares, and light orange triangles, respectively. For each angular region of each FRB, the equivalent widths of the identified sources were averaged to obtain a representative value for that region. A total of 15 FRBs had O VII absorption sources located within the 10-degree region. A Pearson correlation analysis of 15 data points between O VII equivalent width (EW) and DM_{MW} yielded an r -value of 0.8636 and a p -value of 3.35×10^{-5} , indicating a strong linear relationship. Using this correlation, we applied Markov Chain Monte Carlo (MCMC) fitting to derive an empirical relation for estimating DM_{MW} based on the equivalent width of the O VII absorption line:

$$DM_{MW} = (288.71 \pm 73.93) \left(\frac{EW_{O\text{VII}}}{20 \text{ m}\text{\AA}} \right) - (141.17 \pm 50.34) \text{ pc cm}^{-3}. \quad (2)$$

In addition to this analysis, we also examined correlations between the equivalent width of O VIII absorption lines ($EW_{O\text{VIII}}$), and the emission intensities of O VII ($I_{O\text{VII}}$) and O VIII ($I_{O\text{VIII}}$), with DM_{MW} . The equivalent width (EW) reflects the strength of absorption lines, while the emission intensity (I) quantifies the brightness of the corresponding emission lines. The correlations were analyzed across three angular regions for the absorption lines (0° – 10° , 0° – 20° , and 0° – 30°) and for the emission intensities (0° – 5° and 0° – 10°). The results are summarized in Table 2.

Table 2. Pearson Correlation Analysis between DM_{MW} and Absorption/Emission Line Properties (O VII/O VIII Equivalent Width and Emission Intensity) across Different Angular Regions in Galactic Coordinates. Results for alternative analyses to test the robustness of the correlation are also included.

Analysis	Angular Region (degree)	DM_{IGM}	DM_{host} (pc cm^{-3})	R-value	P-value
$EW_{O\text{VII}}$	0° – 10°	Macquart-relation	$30/(1+z)$	0.8636	3.35×10^{-5}
	0° – 20°	Macquart-relation	$30/(1+z)$	0.3436	0.0584
	0° – 30°	Macquart-relation	$30/(1+z)$	0.1029	0.5061
$EW_{O\text{VIII}}$	0° – 10°	Macquart-relation	$30/(1+z)$	-0.2255	0.8552
	0° – 20°	Macquart-relation	$30/(1+z)$	0.2422	0.4041
	0° – 30°	Macquart-relation	$30/(1+z)$	-0.1328	0.5178
$I_{O\text{VII}}$	0° – 5°	Macquart-relation	$30/(1+z)$	0.4849	9.84×10^{-4}
	0° – 10°	Macquart-relation	$30/(1+z)$	0.5396	9.06×10^{-5}
$I_{O\text{VIII}}$	0° – 5°	Macquart-relation	$30/(1+z)$	0.5319	4.92×10^{-4}
	0° – 10°	Macquart-relation	$30/(1+z)$	0.4546	0.0013
* Alternative 1	0° – 10°	Macquart-relation	$60/(1+z)$	0.8512	5.71×10^{-5}
* Alternative 2	0° – 10°	Macquart-relation	$100/(1+z)$	0.8144	2.19×10^{-4}
* Alternative 3	0° – 10°	Macquart-relation	Localization papers ¹	0.8122	2.35×10^{-4}
* Alternative 4 ²	0° – 10°	Macquart-relation	$30/(1+z)$	0.8395	6.36×10^{-4}
* Alternative 5	0° – 10°	Zhang [51]	$30/(1+z)$	0.8630	3.43×10^{-5}

Notes: * All alternative analyses were based on the DM_{MW} and $EW_{O\text{VII}}$ within the 10-degree regions.

¹ For FRBs whose localization papers do not provide DM_{host} , we adopt $30/(1+z)$.

² This analysis excludes 4 unusual FRBs.

3.2. O VIII Absorption

Next, we investigated the relationship between DM_{MW} and O VIII absorption lines. Similar to O VII, O VIII absorption lines can trace hot gas in both the Galactic disk and halo.

We compiled all available O VIII absorption data that use AGN as background sources [3,52–55].

The right panel of Figure 2 shows the correlation between the equivalent width of O VIII absorption lines and DM_{MW} . Similar to the left panel, for each FRB, we searched for O VIII absorption sources within 10, 20, and 30-degree angular regions. However, due to the limited O VIII data, only three FRBs have O VIII absorption data points within the 10-degree region. Even within the 30-degree region, some FRBs lack O VIII absorption sources. Although we performed MCMC fitting and Pearson correlation analysis using data from the 10-degree region, which yielded an r -value of -0.2255 and a p -value of 0.8552, these results are not statistically significant.

3.3. O VII and O VIII Emission

In addition to absorption line data, O VII and O VIII emission line data provide crucial information about the distribution of hot gas in the Milky Way. In this subsection, we discuss the emission line data and their correlation with DM_{MW} , using the most recent dataset published by Pan et al. [56].

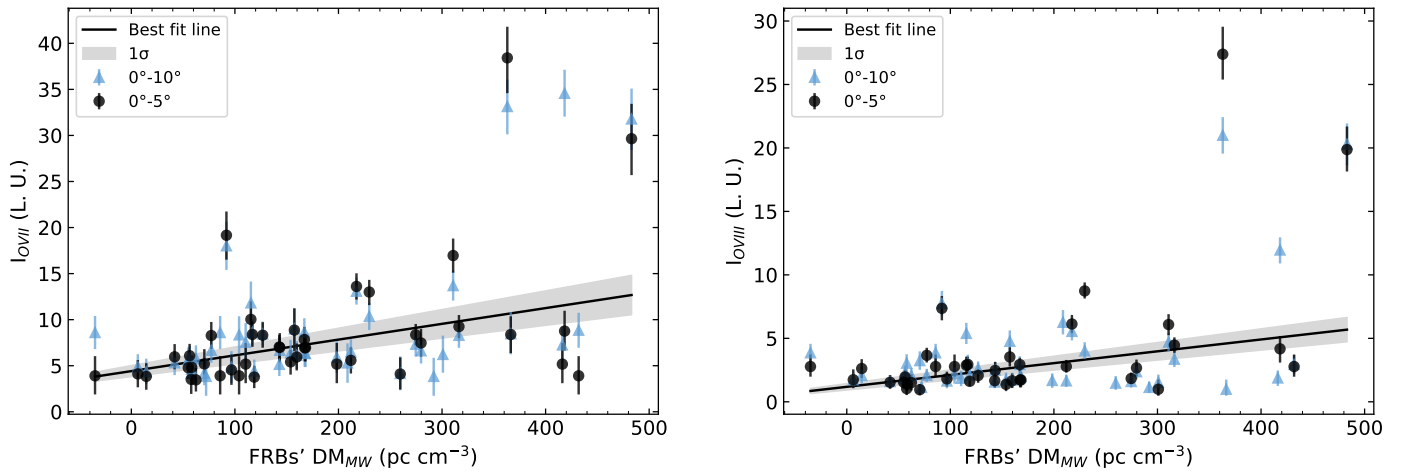


Figure 3. The correlation between DM_{MW} and the emission intensities of O VII (left) and O VIII (right) measured in Line Units (L.U.). For each FRB, black circles and blue triangles represent the average emission intensities within 5-degree and 10-degree angular regions centered on the FRB’s Galactic coordinates (l, b), respectively. The solid lines show the best-fit results obtained from the 5-degree region data for both O VII and O VIII using MCMC fitting. The shaded regions represent the 1σ uncertainty associated with these fits.

Figure 3 illustrates the correlation between the emission intensities of O VII and O VIII (measured in Line Units, L.U.) and DM_{MW} . We averaged the emission data points within 5-degree and 10-degree regions centered on the Galactic coordinates of each FRB. The left panel shows the correlation between O VII emission and DM_{MW} , while the right panel shows the same for O VIII. Black circles represent the average values of data points within the 5-degree region, and blue triangles represent the 10-degree averages. For O VII emission, Pearson correlation analysis on 43 data points within the 5-degree region yielded an r -value of 0.4849 and a p -value of 9.84×10^{-4} . For O VIII, analysis of 39 data points in the 5-degree region gave an r -value of 0.5319 and a p -value of 4.92×10^{-4} . Although both correlations exhibit relatively weak relationships, these correlations are primarily driven by a few outliers with larger values. Therefore, we consider these correlations to be unreliable.

4. Discussion

4.1. Why O VII Absorption Shows the Strongest Correlation

Our analysis reveals that the strongest correlation with DM_{MW} is observed for the O VII absorption line data, as shown in Table 2. This can be attributed to the environment of the Galactic halo, where temperatures around 2×10^6 K are ideal for the presence of highly ionized metals [57]. In this temperature range, O VII becomes the dominant ion, as evidenced by absorption lines detected in the soft X-ray band by observatories such as *Chandra* and *XMM-Newton* [58,59]. Naturally, O VII absorption traces both the hot gas in the Galactic halo and the Galactic disk, reflecting contributions from both components. The high ionization fraction of O VII at these temperatures makes it an effective tracer of the overall hot gas in the Milky Way.

Recent work by Das et al. [50, D21] divided the total DM_{MW} contribution from the Milky Way into four components, corresponding to different gas temperature ranges: cold, cool, warm, and hot phases. Their analysis found that the majority of the DM_{MW} contribution originates from the hot gas phase. Similar to previous studies [e.g., 60–62], they used O VII absorption column density to estimate DM_{MW} . By incorporating key parameters, such as Galactic metallicity and solar oxygen abundance, they developed an empirical formula linking DM_{MW} to the observed O VII absorption.

Following their approach, we used the same formula to convert the relationship into DM versus equivalent width (EW) by assuming Doppler parameters of $b = 50$ km/s and 100 km/s, which are represented in the left panel of Figure 2 by the green and red dashed lines, respectively.

This method aligns closely with our findings, as all three studies emphasize the utility of O VII absorption as a reliable tracer for estimating the Milky Way's DM contribution. Notably, our DM_{MW} data points, also shown in Figure 2, are almost entirely contained within the range defined by these two lines, further supporting the robustness of this approach. These results underscore the critical role of O VII absorption data in tracing the hot gas distribution and quantifying its contribution to the overall DM .

In contrast, the weaker correlation between O VIII and DM_{MW} can be explained by its higher ionization temperature requirement (approximately $10^{6.5}$ K), which is less common in the Galactic halo compared to the 1–2 million K temperature range optimal for O VII. This scarcity of high-temperature gas limits the available data points for O VIII, as evidenced by the small sample of only three FRBs within a 5-degree region. Additionally, O VIII column densities are highly sensitive to the Doppler- b parameter, which is poorly constrained by current observations. In contrast, O VII, which forms more readily under typical halo conditions, serves as a more reliable tracer of the hot gas [see, e.g., 63,64].

Regarding the O VII and O VIII emission lines, although Pearson analysis indicates positive correlations with DM_{MW} , these correlations are weaker compared to those observed for O VII absorption. This discrepancy likely arises because emission lines primarily trace regions of higher density, such as the Galactic disk, which may explain the weaker correlation with the dispersion measure [65].

However, given the small number of localized FRBs, it is important to acknowledge that the limited size of our DM_{MW} sample within 10-degree regions of O VII absorption contributes to the uncertainty in the observed positive correlation. We emphasize that our results merely suggest a potential connection between DM_{MW} and the equivalent width of O VII absorption. Future work, such as that conducted by CHIME/FRB [66], is expected to significantly expand the sample of localized FRBs, facilitating a more reliable and comprehensive analysis of this correlation.

4.2. Comparison with MW Electron Density Distribution Models

In this subsection, we compare the empirically derived DM_{MW} values from our localized FRB sample with DM_{model} predictions from several Milky Way electron density distribution models. These models estimate the Milky Way's contribution to the total dispersion measure based on varying assumptions about the electron distribution. Specifically, we examine the models proposed by Fang et al. [4, F13], Troitsky [67, T17], and Martynenko [68, M22], along with the NE2001 and YMW16 disk models, which provide lower-limit estimates.

Since T17 and M22 primarily focus on describing the electron density distribution in the Galactic halo and do not provide a corresponding disk model, we adopt a disk electron density model that follows a plane-parallel distribution:

$$n_e(z) = n_0 e^{-|z|/z_0} \quad (3)$$

where n_0 and z_0 represent the mid-plane disk electron density and the scale height, respectively. Based on the analysis of 37 pulsar sightlines, Ocker et al. [69, O20] determined best-fit parameters of $n_0 = 0.015 \pm 0.001 \text{ cm}^{-3}$ and $z_0 = 1.57^{+0.15}_{-0.14} \text{ kpc}$, which we adopt here.

Figure 4 illustrates the relationship between DM and Galactic latitude $|b|$. The lines in the figure represent various models of the Milky Way's electron density distribution. YMW16 and NE2001, as the most widely used disk electron density models, are also shown as lower limits.

The model values were calculated at 30-degree intervals in longitude $|l|$, following a longitude range similar to that used by Nakashima et al. [70], and then averaged, with the curves representing these average values. The DM_{MW} sample was divided into 9 bins, each spanning 10 degrees in $|b|$, and is shown as black points. Each point represents the median DM_{MW} value within the corresponding bin, with error bars indicating the 16th and 84th percentiles.

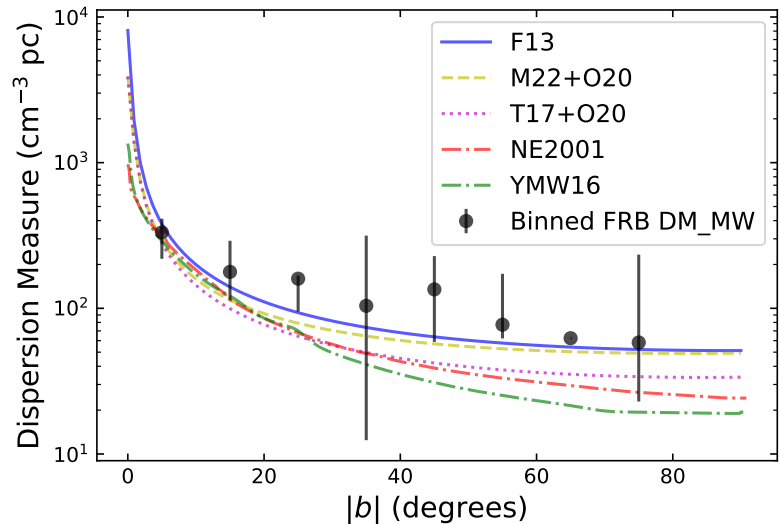


Figure 4. Relationship between DM and $|b|$. The lines represent the three Milky Way electron density distribution models. The solid blue line represents the model by F13, while the pink dotted and yellow dashed lines represent the models by T17 and M22, respectively, both combined with the plane-parallel disk component from O20. The red and green dashdot lines depict two widely used disk electron density models, NE2001 and YMW16, serving as lower limits. Black points indicate the median values of our sample across bins.

Overall, our DM_{MW} values are consistent with the general trend of the models, showing a decrease with increasing $|b|$. Moreover, for disk and halo combination models, such

as F13 and M22+O20, our results demonstrate agreement within the uncertainties. In contrast, for pure disk-only models like NE2001 and YMW16, our DM_{MW} sample exhibits significant excess, emphasizing the contribution of the halo component. We noted that for $|b|$ values between 20 and 50 degrees, DM_{MW} shows a noticeable excess compared to the models, suggesting that the models may not fully capture the complexity of the Milky Way's electron density distribution or that additional factors influence the observed values.

One likely factor is the simplified assumption for the host galaxy contribution, where a constant value of $30/(1+z)$ pc cm⁻³ was used. Such an assumption does not account for the expected variability in the host galaxy's contribution [21]. Additionally, the sparsity of data may also be a contributing factor, for instance, in the $|b|$ range of 50–60 degrees, there are only three data points, which also explains the asymmetry in the error bars.

Furthermore, uncertainties in the Macquart relation used to estimate DM_{IGM} may also contribute to the observed excess. These uncertainties arise from the scatter in the baryon fraction and the distribution of free electrons in the intergalactic medium. Together, these factors could lead to systematic biases in the derived DM_{MW} values.

To address this, we also tested an alternative $DM_{IGM} - z$ relation based on the model from Deng and Zhang [71], using parameters from Zhang [51]. This approach yielded a slightly smaller slope for Equation 2, which could slightly reduce the excess DM_{MW} in comparison to Milky Way electron density models, as presented as Alternative 5 in Table 2. Moreover, we reached the same conclusion that there is a positive correlation between O VII absorption and DM_{MW} .

5. Summary

In this paper, we investigated the total DM_{MW} , which reflects the contributions of the Milky Way's disk and halo to its electron density, using O VII and O VIII absorption and emission data as tracers of the hot, highly ionized gas. Our analysis indicates a positive correlation between O VII absorption and DM_{MW} , from which we derive an empirical relation (Equation 2) to estimate DM_{MW} from the equivalent width of O VII absorption. This relation highlights O VII absorption as a robust tracer of the Milky Way's hot gas and offers a practical tool for future FRB-based studies to constrain the Milky Way's DM contribution.

Our findings also indicate that DM_{MW} reflects contributions from both the disk and halo components of the Milky Way. This conclusion is supported by the weaker correlation between DM_{MW} and O VII/O VIII emission, which primarily traces dense disk regions, and by comparisons with the MW electron density models. The latter shows that DM_{MW} aligns better with models incorporating both disk and halo components, such as F13, M22+O20, but significantly exceeds predictions from pure disk models such as NE2001 and YMW16, emphasizing the importance of the halo's contribution.

Furthermore, the lack of a strong correlation with O VIII absorption suggests that the primary temperature of the Milky Way's hot gas is predominantly around 2×10^6 K, consistent with O VII absorption. While gas at higher temperatures ($3\text{--}5 \times 10^6$ K), typically associated with O VIII absorption, is present, it appears to be less abundant.

In summary, our study highlights the potential of O VII absorption data as a reliable tracer of the Milky Way's hot gas, providing new insights into DM_{MW} contributions. While our results are broadly consistent with previous findings, uncertainties remain, particularly regarding spatial variations in absorption and emission data across different sky regions.

Future studies on FRBs can leverage our empirical formula to estimate DM_{MW} if O VII absorption sources are detected in the vicinity of an FRB. This approach offers a practical tool for the initial localization of FRBs and serves as a stepping stone for further studies on missing baryons. These efforts will not only refine our understanding of Galactic and

extragalactic environments but also advance the broader investigation of FRB sources and the cosmic baryon distribution.

Author Contributions: Data curation, Writing—original draft preparation, Formal analysis, J.W.; Methodology, Z.Z.; Software, X.J.; Conceptualization, Methodology, Supervision, Writing—review and editing, T.F. All authors have read and agreed to the published version of the manuscript.

Conflict of Interest: The authors declare no conflicts of interest.

Data Availability Statement: This study does not include new data. All data used are from previously published sources, as cited in the manuscript.

Funding: J.W., Z.Z., and T.F. were supported by the National Natural Science Foundation of China under Nos. 11890692, 12133008, 12221003. We also acknowledged the science research grant from the China Manned Space Project with No. CMS-CSST-2021-A04.

References

1. Lorimer, D.R.; Bailes, M.; McLaughlin, M.A.; Narkevic, D.J.; Crawford, F. A bright millisecond radio burst of extragalactic origin. *Science* **2007**, *318*, 777–780. <https://doi.org/10.1126/science.1147532>.
2. Shull, J.M.; Smith, B.D.; Danforth, C.W. The baryon census in a multiphase intergalactic medium: 30% of the baryons may still be missing. *The Astrophysical Journal* **2012**, *759*, 23. <https://doi.org/10.1088/0004-637X/759/1/23>.
3. Gupta, A.; Mathur, S.; Krongold, Y.; Nicastro, F.; Galeazzi, M. A huge reservoir of ionized gas around the Milky Way: accounting for the missing mass? *The Astrophysical Journal Letters* **2012**, *756*, L8. <https://doi.org/10.1088/2041-8205/756/1/L8>.
4. Fang, T.; Bullock, J.; Boylan-Kolchin, M. On the hot gas content of the Milky Way halo. *The Astrophysical Journal* **2012**, *762*, 20. <https://doi.org/10.1088/0004-637X/762/1/20>.
5. Nicastro, F.; Krongold, Y.; Fang, T.; Fraternali, F.; Mathur, S.; Bianchi, S.; De Rosa, A.; Piconcelli, E.; Zappacosta, L.; Bischetti, M.; et al. X-Ray Detection of the Galaxy's Missing Baryons in the Circumgalactic Medium of L* Galaxies. *The Astrophysical Journal Letters* **2023**, *955*, L21. <https://doi.org/10.3847/2041-8213/acec70>.
6. Macquart, J.P.; Prochaska, J.; McQuinn, M.; Bannister, K.; Bhandari, S.; Day, C.; Deller, A.; Ekers, R.; James, C.; Marnoch, L.; et al. A census of baryons in the Universe from localized fast radio bursts. *Nature* **2020**, *581*, 391–395. <https://doi.org/10.1038/s41586-020-2300-2>.
7. Cordes, J.M.; Lazio, T.J.W. NE2001. I. A new model for the galactic distribution of free electrons and its fluctuations. *arXiv preprint astro-ph/0207156* **2002**. <https://doi.org/10.48550/arXiv.astro-ph/0207156>.
8. Yao, J.; Manchester, R.; Wang, N. A new electron-density model for estimation of pulsar and FRB distances. *The Astrophysical Journal* **2017**, *835*, 29. <https://doi.org/10.3847/1538-4357/835/1/29>.
9. Price, D.C.; Flynn, C.; Deller, A. A comparison of Galactic electron density models using PyGEDM. *Publications of the Astronomical Society of Australia* **2021**, *38*, e038. <https://doi.org/10.1017/pasa.2021.33>.
10. Gaensler, B.; Madsen, G.; Chatterjee, S.; Mao, S. The vertical structure of warm ionised gas in the Milky Way. *Publications of the Astronomical Society of Australia* **2008**, *25*, 184–200. <https://doi.org/10.1071/AS08004>.
11. Jennings, R.J.; Kaplan, D.L.; Chatterjee, S.; Cordes, J.M.; Deller, A.T. Binary pulsar distances and velocities from gaia data release 2. *The Astrophysical Journal* **2018**, *864*, 26. <https://doi.org/10.3847/1538-4357/aad084>.
12. Platts, E.; Prochaska, J.X.; Law, C.J. A data-driven technique using millisecond transients to measure the milky way halo. *The Astrophysical Journal Letters* **2020**, *895*, L49. <https://doi.org/10.3847/2041-8213/ab930a>.
13. Cook, A.M.; Bhardwaj, M.; Gaensler, B.; Scholz, P.; Eadie, G.M.; Hill, A.S.; Kaspi, V.M.; Masui, K.W.; Curtin, A.P.; Dong, F.A.; et al. An FRB Sent Me a DM: Constraining the Electron Column of the Milky Way Halo with Fast Radio Burst Dispersion Measures from CHIME/FRB. *The Astrophysical Journal* **2023**, *946*, 58. <https://doi.org/10.3847/1538-4357/acbbd0>.
14. Wei, J.J.; Melia, F. Investigating Cosmological Models and the Hubble Tension Using Localized Fast Radio Bursts. *The Astrophysical Journal* **2023**, *955*, 101. <https://doi.org/10.3847/1538-4357/acefb8>.
15. Huang, Y.; Lee, K.G.; Libeskind, N.I.; Simha, S.; Valade, A.; Prochaska, J.X. Modeling the Cosmic Dispersion Measure in the D< 120 Mpc Local Universe. *arXiv preprint arXiv:2410.22098* **2024**. <https://doi.org/10.48550/arXiv.2410.22098>.
16. Smith, R.K.; Bautz, M.W.; Edgar, R.J.; Fujimoto, R.; Hamaguchi, K.; Hughes, J.P.; Ishida, M.; Kelley, R.; Kilbourne, C.A.; Kuntz, K.; et al. Suzaku observations of the local and distant hot ISM. *Publications of the Astronomical Society of Japan* **2007**, *59*, S141–S150. <https://doi.org/10.1093/pasj/59.sp1.S141>.

17. Henley, D.B.; Shelton, R.L. An XMM-Newton survey of the soft X-ray background. III. The galactic halo X-ray emission. *The Astrophysical Journal* **2013**, *773*, 92. <https://doi.org/10.1088/0004-637X/773/2/92>.
18. Nicastro, F.; Kaastra, J.; Krongold, Y.; Borgani, S.; Branchini, E.; Cen, R.; Dadina, M.; Danforth, C.; Elvis, M.; Fiore, F.; et al. Observations of the missing baryons in the warm-hot intergalactic medium. *Nature* **2018**, *558*, 406–409. <https://doi.org/10.1038/s41586-018-0204-1>.
19. Xu, J.; Feng, Y.; Li, D.; Wang, P.; Zhang, Y.; Xie, J.; Chen, H.; Wang, H.; Kang, Z.; Hu, J.; et al. Blinkverse: a database of fast radio bursts. *Universe* **2023**, *9*, 330. <https://doi.org/10.3390/universe9070330>.
20. Kurtz, M.J.; Eichhorn, G.; Accomazzi, A.; Grant, C.S.; Murray, S.S.; Watson, J.M. The NASA astrophysics data system: Overview. *Astronomy and astrophysics supplement series* **2000**, *143*, 41–59. <https://doi.org/10.1016/j.ascom.2024.100879>.
21. Mo, J.F.; Zhu, W.; Wang, Y.; Tang, L.; Feng, L.L. The dispersion measure of Fast Radio Bursts host galaxies: estimation from cosmological simulations. *Monthly Notices of the Royal Astronomical Society* **2023**, *518*, 539–561. <https://doi.org/10.1093/mnras/stac3104>.
22. Niu, C.H.; Aggarwal, K.; Li, D.; Zhang, X.; Chatterjee, S.; Tsai, C.W.; Yu, W.; Law, C.J.; Burke-Spolaor, S.; Cordes, J.M.; et al. A repeating fast radio burst associated with a persistent radio source. *Nature* **2022**, *606*, 873–877. <https://doi.org/10.1038/s41586-022-04755-5>.
23. Bhandari, S.; Gordon, A.C.; Scott, D.R.; Marnoch, L.; Sridhar, N.; Kumar, P.; James, C.W.; Qiu, H.; Bannister, K.W.; Deller, A.T.; et al. A Nonrepeating Fast Radio Burst in a Dwarf Host Galaxy. *The Astrophysical Journal* **2023**, *948*, 67. <https://doi.org/10.3847/1538-4357/acc178>.
24. Ryder, S.D.; Bannister, K.W.; Bhandari, S.; Deller, A.; Ekers, R.; Glowacki, M.; Gordon, A.C.; Gourdji, K.; James, C.; Kilpatrick, C.D.; et al. A luminous fast radio burst that probes the Universe at redshift 1. *Science* **2023**, *382*, 294–299. <https://doi.org/10.1126/science.adf2678>.
25. Connor, L.; Ravi, V.; Catha, M.; Chen, G.; Faber, J.T.; Lamb, J.W.; Hallinan, G.; Harnach, C.; Hellbourg, G.; Hobbs, R.; et al. Deep Synoptic Array science: Two fast radio burst sources in massive galaxy clusters. *The Astrophysical Journal Letters* **2023**, *949*, L26. <https://doi.org/10.3847/2041-8213/acd3ea>.
26. Cordes, J.M.; Ocker, S.K.; Chatterjee, S. Redshift estimation and constraints on intergalactic and interstellar media from dispersion and scattering of fast radio bursts. *The Astrophysical Journal* **2022**, *931*, 88. <https://doi.org/10.3847/1538-4357/ac6873>.
27. Tendulkar, S.P.; Bassa, C.; Cordes, J.M.; Bower, G.C.; Law, C.J.; Chatterjee, S.; Adams, E.A.; Bogdanov, S.; Burke-Spolaor, S.; Butler, B.J.; et al. The host galaxy and redshift of the repeating fast radio burst FRB 121102. *The Astrophysical Journal Letters* **2017**, *834*, L7. <https://doi.org/10.3847/2041-8213/834/2/L7>.
28. Lee-Waddell, K.; James, C.W.; Ryder, S.D.; Mahony, E.K.; Bahramian, A.; Koribalski, B.S.; Kumar, P.; Marnoch, L.; North-Hickey, F.O.; Sadler, E.M.; et al. The host galaxy of FRB 20171020A revisited. *Publications of the Astronomical Society of Australia* **2023**, *40*, e029. <https://doi.org/10.1017/pasa.2023.27>.
29. Bhandari, S.; Heintz, K.E.; Aggarwal, K.; Marnoch, L.; Day, C.K.; Sydnor, J.; Burke-Spolaor, S.; Law, C.J.; Prochaska, J.X.; Tejos, N.; et al. Characterizing the fast radio burst host galaxy population and its connection to transients in the local and extragalactic universe. *The Astronomical Journal* **2022**, *163*, 69. <https://doi.org/10.3847/1538-3881/ac3aec>.
30. Marcote, B.; Nimmo, K.; Hessels, J.; Tendulkar, S.; Bassa, C.; Paragi, Z.; Keimpema, A.; Bhardwaj, M.; Karuppusamy, R.; Kaspi, V.; et al. A repeating fast radio burst source localized to a nearby spiral galaxy. *Nature* **2020**, *577*, 190–194. <https://doi.org/10.1038/s41586-019-1866-z>.
31. Bannister, K.W.; Deller, A.T.; Phillips, C.; Macquart, J.P.; Prochaska, J.X.; Tejos, N.; Ryder, S.D.; Sadler, E.M.; Shannon, R.M.; Simha, S.; et al. A single fast radio burst localized to a massive galaxy at cosmological distance. *Science* **2019**, *365*, 565–570. <https://doi.org/10.1126/science.aaw5903>.
32. Bhardwaj, M.; Kirichenko, A.Y.; Michilli, D.; Mayya, Y.; Kaspi, V.; Gaensler, B.; Rahman, M.; Tendulkar, S.; Fonseca, E.; Josephy, A.; et al. A local universe host for the repeating fast radio burst FRB 20181030A. *The Astrophysical Journal Letters* **2021**, *919*, L24. <https://doi.org/10.3847/2041-8213/ac223b>.
33. Prochaska, J.X.; Macquart, J.P.; McQuinn, M.; Simha, S.; Shannon, R.M.; Day, C.K.; Marnoch, L.; Ryder, S.; Deller, A.; Bannister, K.W.; et al. The low density and magnetization of a massive galaxy halo exposed by a fast radio burst. *Science* **2019**, *366*, 231–234. <https://doi.org/10.1126/science.aay0073>.
34. Bhardwaj, M.; Michilli, D.; Kirichenko, A.Y.; Modilim, O.; Shin, K.; Kaspi, V.M.; Andersen, B.C.; Cassanelli, T.; Brar, C.; Chatterjee, S.; et al. Host galaxies for four nearby CHIME/FRB sources and the local universe FRB host galaxy population. *The Astrophysical Journal Letters* **2024**, *971*, L51. <https://doi.org/10.3847/2041-8213/ad64d1>.
35. Ravi, V.; Catha, M.; D’addario, L.; Djorgovski, S.; Hallinan, G.; Hobbs, R.; Kocz, J.; Kulkarni, S.; Shi, J.; Vedantham, H.; et al. A fast radio burst localized to a massive galaxy. *Nature* **2019**, *572*, 352–354. <https://doi.org/10.1038/s41586-019-1389-7>.
36. Heintz, K.E.; Prochaska, J.X.; Simha, S.; Platts, E.; Fong, W.f.; Tejos, N.; Ryder, S.D.; Aggerwal, K.; Bhandari, S.; Day, C.K.; et al. Host galaxy properties and offset distributions of fast radio bursts: implications for their progenitors. *The Astrophysical Journal* **2020**, *903*, 152. <https://doi.org/10.3847/1538-4357/abb6fb>.

37. Kirsten, F.; Marcote, B.; Nimmo, K.; Hessels, J.; Bhardwaj, M.; Tendulkar, S.; Keimpema, A.; Yang, J.; Snelders, M.; Scholz, P.; et al. A repeating fast radio burst source in a globular cluster. *Nature* **2022**, *602*, 585–589. <https://doi.org/10.1038/s41586-021-04354-w>.
38. Rajwade, K.; Bezuidenhout, M.C.; Caleb, M.; Driessen, L.; Jankowski, F.; Malenta, M.; Morello, V.; Sanidas, S.; Stappers, B.; Surnis, M.; et al. First discoveries and localizations of Fast Radio Bursts with MeerTRAP: real-time, commensal MeerKAT survey. *Monthly Notices of the Royal Astronomical Society* **2022**, *514*, 1961–1974. <https://doi.org/10.1093/mnras/stac1450>.
39. Fong, W.f.; Dong, Y.; Leja, J.; Bhandari, S.; Day, C.K.; Deller, A.T.; Kumar, P.; Prochaska, J.X.; Scott, D.R.; Bannister, K.W.; et al. Chronicling the host galaxy properties of the remarkable repeating FRB 20201124A. *The Astrophysical Journal Letters* **2021**, *919*, L23. <https://doi.org/10.3847/2041-8213/ac242b>.
40. Gordon, A.C.; Fong, W.f.; Kilpatrick, C.D.; Eftekhari, T.; Leja, J.; Prochaska, J.X.; Nugent, A.E.; Bhandari, S.; Blanchard, P.K.; Caleb, M.; et al. The Demographics, Stellar Populations, and Star Formation Histories of Fast Radio Burst Host Galaxies: Implications for the Progenitors. *The Astrophysical Journal* **2023**, *954*, 80. <https://doi.org/10.3847/1538-4357/ace5aa>.
41. Driessen, L.N.; Barr, E.; Buckley, D.; Caleb, M.; Chen, H.; Chen, W.; Gromadzki, M.; Jankowski, F.; Kraan-Korteweg, R.; Palmerio, J.; et al. FRB 202104051: a nearby Fast Radio Burst localized to sub-arcsecond precision with MeerKAT. *Monthly Notices of the Royal Astronomical Society* **2024**, *527*, 3659–3673. <https://doi.org/10.1093/mnras/stad3329>.
42. Caleb, M.; Driessen, L.; Gordon, A.; Tejos, N.; Bernales, L.; Qiu, H.; Chibueze, J.; Stappers, B.; Rajwade, K.; Cavallaro, F.; et al. A subarcsec localized fast radio burst with a significant host galaxy dispersion measure contribution. *Monthly Notices of the Royal Astronomical Society* **2023**, *524*, 2064–2077. <https://doi.org/10.1093/mnras/stad1839>.
43. Glowacki, M.; Lee-Waddell, K.; Deller, A.; Deg, N.; Gordon, A.; Grundy, J.; Marnoch, L.; Shen, A.; Ryder, S.; Shannon, R.; et al. WALLABY Pilot Survey: H i in the Host Galaxy of a Fast Radio Burst. *The Astrophysical Journal* **2023**, *949*, 25. <https://doi.org/10.3847/1538-4357/acc1e3>.
44. Law, C.J.; Sharma, K.; Ravi, V.; Chen, G.; Catha, M.; Connor, L.; Faber, J.T.; Hallinan, G.; Harnach, C.; Hellbourg, G.; et al. Deep Synoptic Array Science: First FRB and Host Galaxy Catalog. *arXiv preprint arXiv:2307.03344* **2023**. <https://doi.org/10.48550/arXiv.2307.03344>.
45. Ravi, V.; Catha, M.; Chen, G.; Connor, L.; Cordes, J.M.; Faber, J.T.; Lamb, J.W.; Hallinan, G.; Harnach, C.; Hellbourg, G.; et al. Deep Synoptic Array science: a 50 Mpc fast radio burst constrains the mass of the Milky Way circumgalactic medium. *arXiv preprint arXiv:2301.01000* **2023**. <https://doi.org/10.48550/arXiv.2301.01000>.
46. Ravi, V.; Catha, M.; Chen, G.; Connor, L.; Faber, J.T.; Lamb, J.W.; Hallinan, G.; Harnach, C.; Hellbourg, G.; Hobbs, R.; et al. Deep Synoptic Array Science: Discovery of the Host Galaxy of FRB 20220912A. *The Astrophysical Journal Letters* **2023**, *949*, L3. <https://doi.org/10.3847/2041-8213/acc4b6>.
47. Glowacki, M.; Bera, A.; Lee-Waddell, K.; Deller, A.; Dial, T.; Gourdjji, K.; Simha, S.; Caleb, M.; Marnoch, L.; Prochaska, J.X.; et al. H i, FRB, What's Your z: The First FRB Host Galaxy Redshift from Radio Observations. *The Astrophysical Journal Letters* **2024**, *962*, L13. <https://doi.org/10.3847/2041-8213/ad1f62>.
48. Fang, T.; Buote, D.; Bullock, J.; Ma, R. XMM-NEWTON SURVEY OF LOCAL ABSORPTION LINES IN THE SPECTRA OF ACTIVE GALACTIC NUCLEI. *The Astrophysical Journal Supplement Series* **2015**, *217*, 21. <https://doi.org/10.1088/0067-0049/217/2/21>.
49. Longinotti, A.; Costantini, E.; Petrucci, P.; Boisson, C.; Mouchet, M.; Santos-Lleo, M.; Matt, G.; Ponti, G.; Gonçalves, A. High-resolution X-ray spectroscopy of the Seyfert 1 Mrk 841: insights into the warm absorber and warm emitter. *Astronomy & Astrophysics* **2010**, *510*, A92. <https://doi.org/10.1051/0004-6361/200912925>.
50. Das, S.; Mathur, S.; Gupta, A.; Nicastro, F.; Krongold, Y. Empirical estimates of the Galactic halo contribution to the dispersion measures of extragalactic fast radio bursts using X-ray absorption. *Monthly Notices of the Royal Astronomical Society* **2021**, *500*, 655–662. <https://doi.org/10.1093/mnras/staa3299>.
51. Zhang, B. Fast radio burst energetics and detectability from high redshifts. *The Astrophysical Journal Letters* **2018**, *867*, L21. <https://doi.org/10.3847/2041-8213/aae8e3>.
52. Zappacosta, L.; Nicastro, F.; Maiolino, R.; Tagliaferri, G.; Buote, D.; Fang, T.; Humphrey, P.; Gastaldello, F. Studying the WHIM content of large-scale structures along the line of sight to H 2356-309. *The Astrophysical Journal* **2010**, *717*, 74. <https://doi.org/10.1088/0004-637X/717/1/74>.
53. Fang, T.; Jiang, X. High resolution X-ray spectroscopy of the local hot gas along the 3C 273 sightline. *The Astrophysical Journal Letters* **2014**, *785*, L24. <https://doi.org/10.1088/2041-8205/785/2/L24>.
54. Bonamente, M.; Nevalainen, J.; Tilton, E.; Liivamägi, J.; Tempel, E.; Heinämäki, P.; Fang, T. A possible Chandra and Hubble Space Telescope detection of extragalactic WHIM towards PG 1116+ 215. *Monthly Notices of the Royal Astronomical Society* **2016**, *457*, 4236–4247. <https://doi.org/10.1093/mnras/stw285>.
55. Das, S.; Mathur, S.; Nicastro, F.; Krongold, Y. Discovery of a very hot phase of the Milky Way circumgalactic medium with non-solar abundance ratios. *The Astrophysical Journal Letters* **2019**, *882*, L23. <https://doi.org/10.3847/2041-8213/ab3b09>.
56. Pan, Z.; Qu, Z.; Bregman, J.N.; Liu, J. The XMM-Newton Line Emission Analysis Program (X-LEAP). I. Emission-line Survey of O vii, O viii, and Fe L-shell Transitions. *The Astrophysical Journal Supplement Series* **2024**, *271*, 62. <https://doi.org/10.3847/1538-4365/ad2ea0>.

57. Kaaret, P.; Koutroumpa, D.; Kuntz, K.; Jahoda, K.; Bluem, J.; Gulick, H.; Hodges-Kluck, E.; LaRocca, D.; Ringuette, R.; Zajczyk, A. A disk-dominated and clumpy circumgalactic medium of the Milky Way seen in X-ray emission. *Nature Astronomy* **2020**, *4*, 1072–1077. <https://doi.org/10.1038/s41550-020-01215-w>.
58. Nicastro, F.; Mathur, S.; Elvis, M.; Drake, J.; Fang, T.; Fruscione, A.; Krongold, Y.; Marshall, H.; Williams, R.; Zezas, A. The mass of the missing baryons in the X-ray forest of the warm-hot intergalactic medium. *nature* **2005**, *433*, 495–498. <https://doi.org/10.1038/nature03245>.
59. Bregman, J.N.; Lloyd-Davies, E.J. X-Ray absorption from the Milky Way halo and the local group. *The Astrophysical Journal* **2007**, *669*, 990. <https://doi.org/10.1086/521321>.
60. Shull, J.M.; Danforth, C.W. The Dispersion of Fast Radio Bursts from a Structured Intergalactic Medium at Redshifts $z < 1.5$. *The Astrophysical Journal Letters* **2018**, *852*, L11. <https://doi.org/10.3847/2041-8213/aaa2fa>.
61. Prochaska, J.X.; Zheng, Y. Probing Galactic haloes with fast radio bursts. *Monthly Notices of the Royal Astronomical Society* **2019**, *485*, 648–665. <https://doi.org/10.1093/mnras/stz261>.
62. Yamasaki, S.; Totani, T. The galactic halo contribution to the dispersion measure of extragalactic fast radio bursts. *The Astrophysical Journal* **2020**, *888*, 105. <https://doi.org/10.3847/1538-4357/ab58c4>.
63. Mathur, S.; Weinberg, D.H.; Chen, X. Tracing the warm-hot intergalactic medium at low redshift: X-ray forest observations toward H1821+ 643. *The Astrophysical Journal* **2003**, *582*, 82. <https://doi.org/10.1086/344509>.
64. Williams, R.J.; Mathur, S.; Nicastro, F.; Elvis, M.; Drake, J.J.; Fang, T.; Fiore, F.; Krongold, Y.; Wang, Q.D.; Yao, Y. Probing the local group medium toward Markarian 421 with Chandra and the far ultraviolet spectroscopic explorer. *The Astrophysical Journal* **2005**, *631*, 856. <https://doi.org/10.1086/431343>.
65. Henley, D.B.; Shelton, R.L. An XMM-Newton survey of the soft X-ray background. II. An all-sky catalog of diffuse O VII and O VIII emission intensities. *The Astrophysical Journal Supplement Series* **2012**, *202*, 14. <https://doi.org/10.1088/0067-0049/202/2/14>.
66. Amiri, M.; Bandura, K.; Berger, P.; Bhardwaj, M.; Boyce, M.; Boyle, P.; Brar, C.; Burhanpurkar, M.; Chawla, P.; Chowdhury, J.; et al. The CHIME fast radio burst project: system overview. *The Astrophysical Journal* **2018**, *863*, 48. <https://doi.org/10.3847/1538-4357/aad188>.
67. Troitsky, S. Density and metallicity of the Milky Way circumgalactic gas. *Monthly Notices of the Royal Astronomical Society: Letters* **2017**, *468*, L36–L40. <https://doi.org/10.1093/mnrasl/slx022>.
68. Martynenko, N. Constraining density and metallicity of the Milky Way's hot gas halo from O VII spectra and ram-pressure stripping. *Monthly Notices of the Royal Astronomical Society* **2022**, *511*, 843–858. <https://doi.org/10.1093/mnras/stac164>.
69. Ocker, S.K.; Cordes, J.M.; Chatterjee, S. Electron density structure of the local galactic disk. *The Astrophysical Journal* **2020**, *897*, 124. <https://doi.org/10.3847/1538-4357/ab98f9>.
70. Nakashima, S.; Inoue, Y.; Yamasaki, N.; Sofue, Y.; Kataoka, J.; Sakai, K. Spatial distribution of the Milky Way hot gaseous halo constrained by Suzaku X-ray observations. *The Astrophysical Journal* **2018**, *862*, 34. <https://doi.org/10.3847/1538-4357/aaccebb>.
71. Deng, W.; Zhang, B. Cosmological implications of fast radio burst/gamma-ray burst associations. *The Astrophysical Journal Letters* **2014**, *783*, L35. <https://doi.org/10.1088/2041-8205/783/2/L35>.

Disclaimer/Publisher's Note: The statements, opinions and data contained in all publications are solely those of the individual author(s) and contributor(s) and not of MDPI and/or the editor(s). MDPI and/or the editor(s) disclaim responsibility for any injury to people or property resulting from any ideas, methods, instructions or products referred to in the content.